

Supporting the Detection of Early Alzheimer's Disease with a Four-Channel EEG Analysis

Eduardo Perez-Valero^{*,†}, Christian Morillas^{*,§}, Miguel A. Lopez-Gordo^{†,¶}
and Jesus Minguillon^{†,||}

**Department of Computer Engineering, Automation and Robotics
and Research Centre for Information
and Communications Technologies, University of Granada
Periodista Daniel Saucedo Aranda, Granada 18071, Spain*

*†Department of Signal Theory, Telematics
and Communications and Research Centre for Information
and Communications Technologies, University of Granada
Periodista Daniel Saucedo Aranda, Granada 18071, Spain*

‡edu@ugr.es

§cmg@ugr.es

¶malg@ugr.es

||minguillon@ugr.es

Accepted 19 January 2023

Published Online 16 February 2023

Alzheimer's disease (AD) is the most prevalent form of dementia. Although there is no current cure, medical treatment can help to control its progression. Hence, early-stage diagnosis is crucial to maximize the living standards of the patients. Biochemical markers and medical imaging in combination with neuropsychological tests represent the most extended diagnosis procedure. However, these techniques require specialized personnel and long processing time. Furthermore, the access to some of these techniques is often limited in crowded healthcare systems and rural areas. In this context, electroencephalography (EEG), a non-invasive technique to obtain endogenous brain information, has been proposed for the diagnosis of early-stage AD. Despite the valuable information provided by clinical EEG and high density montages, these approaches are impractical in conditions such as those described above. Consequently, in this study, we evaluated the feasibility of using a reduced EEG montage with only four channels to detect early-stage AD. For this purpose, we involved eight clinically diagnosed AD patients and eight healthy controls. The results we obtained reveal similar accuracies (p -value = 0.66) for the reduced montage (0.86) and a 16-channel montage (0.87). This suggests that a four-channel wearable EEG system could be an effective tool for supporting early-stage AD detection.

Keywords: Alzheimer's disease; reduced EEG montage; wearable EEG; automated detection; artificial intelligence.

^{||}Corresponding author.

This is an Open Access article published by World Scientific Publishing Company. It is distributed under the terms of the Creative Commons Attribution-NonCommercial-NoDerivatives 4.0 (CC BY-NC-ND) License which permits use, distribution and reproduction, provided that the original work is properly cited, the use is non-commercial and no modifications or adaptations are made.

1. Introduction

Alzheimer's disease (AD) is the most common form of dementia. This neuro-degenerative pathology involves a series of symptoms at the cognitive and emotional levels, such as memory loss, language deterioration, or mood changes. According to the World Health Organization, dementia affects more than 55 million people worldwide, and prevalence will increase to 78 million by 2030.¹ Since AD represents 60–70% of dementia cases, this means that around 50 million people are expected to live with AD by then. With regard to the costs associated to the disease, the estimated direct medical and social care costs will surpass USD 1.68 trillion by 2030. Unfortunately, at present there is no cure for AD, however, the progression of the disease can be controlled through clinical treatment, thus improving the quality of life of the patients. Therefore, accurate detection during the early stages is one of the main aims in AD care.²

The most accepted techniques for AD detection at the clinical level are those based on the detection of amyloid plaques^{3,4} and neurofibrillary tangles.^{5,6} This is typically performed through the analysis of biochemical markers extracted from cerebro-spinal fluid (CSF)^{7–9} or the processing of medical images (single-photon emission computed tomography,¹⁰ magnetic resonance imaging,¹¹ or positron emission tomography¹²). Nonetheless, both approaches present some drawbacks. On the one hand, the analysis of biochemical markers involves risks associated to the invasiveness of the procedure for extracting the cerebro-spinal fluid (infections, tissue damage, patient reluctance, etc.). On the other hand, the efficacy of image-based techniques is limited for the detection of early-stage AD, although their combination with artificial intelligence algorithms has been proven to be more effective.^{10,11,13,14} In addition to these limitations, the main disadvantage of these techniques towards the detection of early-stage AD is the long sample acquisition and processing times, which prolongs detection times and contributes to growing clinical waiting lists.

Neuropsychological tests are another relevant tool extensively utilized in AD clinical practice. These tests are considered as the gold-standard for the detection of cognitive impairment, which is essential for dementia diagnosis. They evaluate

the performance in different cognitive areas, such as orientation, memory, and language. The Montreal cognitive assessment¹⁵ and the mini-mental state examination¹⁶ are the most widespread assessments. Nonetheless, these tests can be influenced by factors such as visual pathologies, educational level, and emotional state, which may impact their reliability.^{17,18}

As a complementary alternative to the methods relying on biochemical markers, medical imaging, and neuropsychological tests, some authors have proposed other approaches based on electroencephalography (EEG)^{19–26} and magnetoencephalography^{27–29} (MEG). EEG analysis leans on endogenous information and its acquisition and processing times are reduced compared to methods based on biochemical markers and medical imaging. Although this technique cannot provide etiological information, EEG studies have demonstrated the effects produced by AD in brain electrical activity. Such effects have been evidenced in spectral power,^{30,31} complexity,^{32,33} connectivity,^{34,35} or event-related potentials,^{36,37} among other features.

Recent EEG approaches often consist in processing the resting state brain activity and applying machine learning algorithms^{16,22,38–46} and have shown classification accuracies above 80%.^{17,20,21,47} Subsequently, EEG represents a valuable alternative to support AD detection before standard medical techniques are applied to render a comprehensive diagnosis. Particularly, the application of approaches based on resting state EEG and machine learning could be advantageous in neurology or even primary care services. Frequently, healthcare systems are crowded, which reduces the span of medical checks and limits access to medical trials, mainly in low and mid-income countries, and rural areas. In this respect, clinical EEG and high density montages report valuable diagnostic information, and multiple works have demonstrated their relevance for connectivity,⁴⁸ source localization^{49,50} and other analyses. Nonetheless, they are limited in terms of usability considering the scenario described above. This is partially due to the number of electrodes typically used, which often ranges between 64 and 128. Additionally, clinical EEG often requires trained personnel and dedicated facilities, which makes these approaches impractical for primary care services.

In this context, we conceived a scenario where clinicians may potentially detect early-stage AD during a short resting state session using a minimal EEG system. For this, the EEG montage must meet comfort and portability standards similar to those from daily-life wearable devices. As an initial step in this direction, in this work we present a study whose main goal is to investigate the feasibility of detecting early-stage AD from a reduced selection of four EEG channels. For this purpose, we recorded the resting state EEG activity of a group of AD patients and healthy controls using a 16-channel montage. Then, we estimated an accumulated score per channel based on the statistical differences between the EEG features of both groups. Using this score, we elucidated the four-channel selection, which we refer to as reduced montage. With this paper, we extend our previous work² by analyzing the statistical differences in the EEG relative power and complexity of the two groups studied. We also compare the classification performance of the four-channel and the original 16-channel montages. Importantly, the goal of this study is not to investigate AD etiology, nor to find the optimal channel selection in terms of classification, but to assess the feasibility of a four-channel selection that could be included in a wearable minimal montage for early-stage AD detection.

2. Materials and Methods

2.1. Participants

Sixteen participants (AD patients and controls) took part in this study. The participants were recruited by neurologists from the Cognitive and Behavioral Neurology Unit at Hospital Universitario Virgen de las Nieves (HUVN) de Granada (Spain). None of the participants were under a medical treatment that could alter their EEG activity nor affected by other neurological diseases. The AD group included eight participants (five females, three males, mean age 68.8 ± 4.9), and the control group included eight healthy age-matched controls (seven females, one male, mean age 67.0 ± 3.5). The participants in the patient group were cataloged as early AD by the neurologists based on two evaluations: (a) a validated neuropsychological test battery especially adapted to the local population^{51–53} and (b) a CSF or a PET-amyloid analysis following memory complaints during the year prior to the start of this study.

For PET-based detection, trained nuclear medicine specialists used 18F-florbetaben to analyze the scans. Then, they reported the scans as positive or negative depending on the presence of amyloid plaques. The doubtful cases were discussed by the specialists and a final decision was adopted by consensus. For CSF-based detection (total- τ , A β 42, and τ -phosphorylated fraction), CSF was extracted through lumbar puncture utilizing a syringe and a 20-gauge needle. Two independent laboratories performed the CSF analysis. Subsequently, the analysis results were encoded as pathological or normal. Considering this, the AD patients either tested positive for amyloid plaques in the PET scan or yielded pathological results in the CSF analysis.

This study was conducted at HUVN after protocol approval by the ethics committee. The participants signed an informed consent document prior to the experimental session, and members of the hospital staff monitored them throughout the whole study.

2.2. EEG acquisition and pre-processing

We recorded the EEG activity of the participants for six minutes while they were comfortably resting in a chair (resting state) with their eyes open. For this purpose, we used the Versatile EEG acquisition device by Bitbrain (Zaragoza, Spain), which works at a sampling frequency of 256 Hz and provides support for 16 channels. Regarding the montage, we performed the acquisition using 16 positions of the 10–20 International System (see Fig. 1(a)). The ground electrode was located in the AFz position, whilst we set the reference at the left ear lobe. The sensors used were semi-dry, and during the recordings, the skin-sensor impedance was kept in the appropriate range through the real-time impedance monitoring feature of the acquisition software.

We pre-processed the recordings offline according to the procedure described in Refs. 2, 54 and 55 (see Fig. 1(b)). First, we filtered the raw EEG signals using a FIR bandpass filter with 1–45 Hz passband and zero phase-shift. Then, we split the filtered signals into four-second segments (epochs) without overlapping. This epoch length is in a range typically adopted in the literature.³⁸ Finally, we applied artifact rejection using Autoreject and independent component analysis (ICA) and we normalized the epochs to unit mean. Autoreject is a data-based algorithm

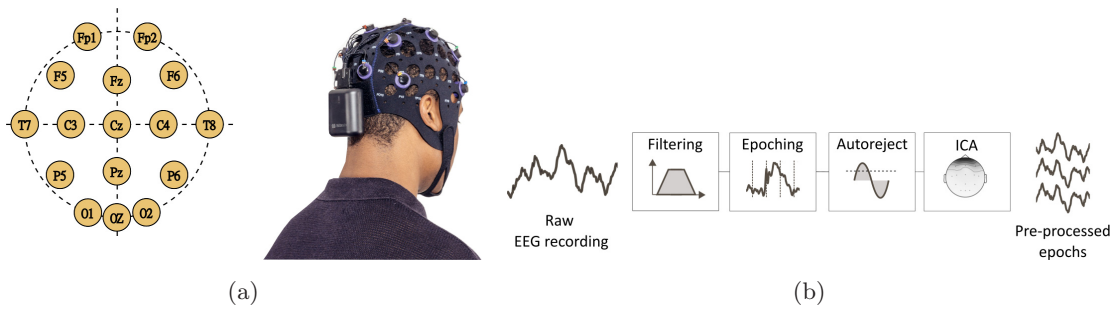


Fig. 1. (a) Channel montage (left) and versatile EEG recording system by Bitbrain (right) utilized in this study for the EEG acquisition. (b) Pre-processing pipeline of the raw EEG.

designed to find an amplitude threshold for each channel in order to identify and reject artifactual signal segments.⁵⁶ Additionally, we applied ICA to reject artifacts related to eye blinks. This algorithm is often applied in the EEG literature to find and reject artifactual components like blinks.⁵⁷ We automatically identified the blink component based on a correlation analysis of the components' time series and the time series of the prefrontal channel Fp1, which is the location where most of the blink energy is captured (excepting electrooculogram channels). Thereby, Fp1 acted as an electrooculogram proxy. Then, we reconstructed the EEG without the blink component.

2.3. Relative power features

The relative power of a signal in a frequency band represents the proportion of the total signal power that is contained in the range of the band. We included the relative power in our analysis because resting state EEG slowing is a well-known effect in AD patients.⁵⁸ Slowing translates into an increase of the relative power in the delta and theta bands, coupled with a decrease of the relative power in the alpha and beta bands. Equation (1) shows the formula for the relative power.

$$\text{RP} = \frac{\sum_{f_{\text{ini}}}^{f_{\text{end}}} P}{\sum_{\forall f} P}, \quad (1)$$

RP stands for relative power, f_{ini} and f_{end} represent the boundaries of the band where the relative power is estimated, and P represents power.

For this study, we extracted the relative power in delta (1–4 Hz), theta (4–8 Hz), alpha (8–13 Hz), beta (13–30 Hz), and lower gamma (30–45 Hz). Hence, we extracted a total of 80 relative power features per

epoch (corresponding to 16 channels and five bands). To extract the relative power, we utilized the `compute_pow_freq_bands` function in the MNE Python package with the default input parameters, which estimates the relative power using Welch's method with a Hamming window and no overlap.

2.4. Complexity features

We extracted two complexity features for each epoch: spectral entropy and Hjorth complexity. We included these two complexity features in our analysis because a decrease in EEG complexity is another widely reported effect in AD patients in the literature.^{38,59}

Spectral entropy represents the Shannon entropy of the power spectra of a signal. It describes the power spectra distribution uniformity, and therefore, the regularity of the EEG. Consequently, spectral entropy is maximal for white noise (very uniform power spectra), and minimal for a pure sine wave (very narrow power spectra). Equation (2) represents the spectral entropy.

$$\text{SE} = - \sum_f S(f) \cdot \log_2 S(f), \quad (2)$$

SE stands for spectral entropy, f for the frequencies in the spectral range of the signal, and S for the normalized signal spectrum.

On the other hand, Hjorth complexity is one of the three Hjorth parameters (activity, mobility, and complexity). This feature compares the similarity of a signal to a pure sine wave and augments with signal regularity. Equation (3) represents the Hjorth complexity.

$$\text{HC} = \frac{\sigma_s''/\sigma_s'}{\sigma_s'/\sigma_s}, \quad (3)$$

HC stands for Hjorth complexity, and σ_s , σ'_s and σ''_s stand for the standard deviation of the EEG signal, and of its first and second derivatives.

Since we extracted the two complexity features described in this subsection for each channel individually, we obtained 32 complexity features per epoch. To extract the two features described in this subsection, we also utilized the MNE Python package.

2.5. Statistical analysis

The feature extraction procedure yielded a total of 112 features per epoch. This corresponds to 80 relative power features (corresponding to 16 channels and five bands) and 32 complexity features (corresponding to sixteen channels and two complexity metrics).

With this in mind, we evaluated the statistical differences between AD patients and controls feature by feature. To do so, for each participant, we averaged all the features across the epochs. Thereby, we ended up with a single observation for each feature per participant and channel. Then, for each feature, we grouped the observations into two independent samples: AD patients and controls, and we applied an independent samples t -test. This test was preceded by a Shapiro–Wilk test to assess the normality of the distributions. For all the statistical analyses, we set the significance threshold at 5% ($\alpha = 0.05$). Since for each feature we compared the group distributions across 16 channels, we applied multiple comparison correction using the Benjamini and Hochberg method.⁶⁰

Additionally, we evaluated the differences between the AD and control groups for the average relative power and complexity across the scalp. For this purpose, we averaged the single-observation features across channels. For instance, for the spectral entropy, we started with 16 features (one per channel), and we averaged them to obtain a single spectral entropy value for the scalp. Then, we applied an independent samples t -test to evaluate the differences between the two groups. We applied the method referred in the previous paragraph for multiple comparison correction.

Subsequently, we identified those channels where the differences between the two groups were most significant. To do so, we estimated the relative univariate score for each feature using the p -value from

the corresponding t -test. Concretely, in order for this score to be inversely proportional to the p -value, we estimated the relative univariate feature score as indicated by Eq. (4).

$$FS(x) = \frac{-\log_{10}p_{\text{value}}(x)}{\max(-\log_{10}p_{\text{values}})}, \quad (4)$$

$FS(x)$ represents the relative univariate feature score for a particular feature x , (e.g. Hjorth complexity at channel Cz); $p_{\text{value}}(x)$ represents the p -value obtained for the comparison of the distribution of feature x across the two study groups; and the denominator is a scaling factor applied in order for the FS to range from 0 to 1.

Then, we obtained a single score per channel by summing the scores of all the features from each channel and we represented the channel scores in a topographical map. Lastly, we used these scores to select the channels for the reduced montage. To assess the performance of the original and the reduced montage, we compared their performance in terms of the average classification accuracy, the confusion matrices, and the ROC curves. Furthermore, we applied a Mann–Whitney test to evaluate the statistical differences between them. We applied this test because the distributions compared did not meet the assumptions for a parametric test.

2.6. Classification of AD versus controls

Following feature extraction, we created the feature matrix for the AD versus controls classification problem. First, for each participant, we arranged the extracted features in a matrix with epochs in the rows and features in the columns. As outlined in subsections 2.5, for each participant, we extracted 112 features per epoch. Then, to increase the signal-to-noise ratio, we followed the procedure described in Refs. 2 and 61 and we averaged every six succeeding epochs. Beyond this point, the rows of the feature matrix no longer represented individual epochs, but the average of every six consecutive epochs. Nonetheless, for readability, we will refer to the rows of the feature matrix as epochs throughout the rest of this work. Finally, we concatenated the matrices of all the participants to create the feature matrix for the classification problem.

Subsequently, we set a classification pipeline that included a feature scaler and a classifier. We examined three classifiers: a logistic regressor (LR), a support vector machine (SVM) with radial basis function kernel, and a multi-layer perceptron (MLP). We selected these classifiers because they have been widely utilized in the literature.³⁸ For the mentioned classifiers, we evaluated the following hyperparameters: the inverse of the regularization strength (C), the weights of the classes (class weight), and the penalty term (penalty) for the LR, the regularization strength (C), and the kernel coefficient (gamma) for the SVM, and finally, the activation function (activation), the regularization strength (alpha), and the hidden layer sizes (hidden layers), for the MLP.

To evaluate these classifiers, we applied the *Grid-SearchCV* function from the open-source Python package Scikit-learn. This function performs grid-search (in order to obtain the best classifier hyperparameters) and cross-validation (to evaluate the performance of the classifiers). Since the classification problem assessed in this work involves the discrimination of participants from clinical groups, we followed a leave-one-subject-out (LOSO) strategy for the cross-validation (see Fig. 2). This cross-validation strategy works as follows: first, the dataset is partitioned into as many folds as participants; then, an iterative procedure is conducted for as many

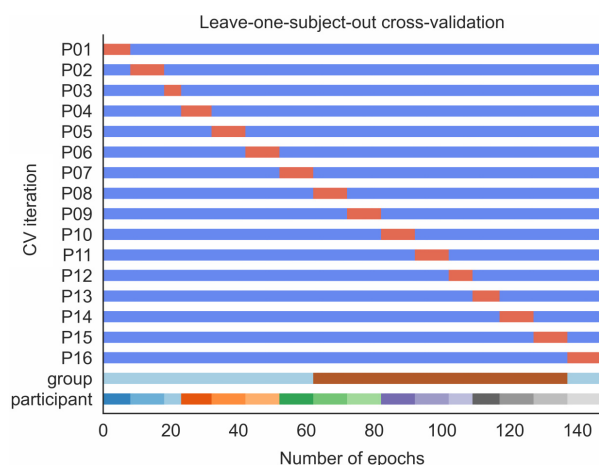


Fig. 2. Cross-validation strategy adopted in this study. For each iteration, the train set (in blue) holds the data of all the participants but one, which is held out for testing (in red). The last two rows represent the group (AD in light blue and control in brown), and the epochs of each participant.

iterations as folds; for each iteration, the classifier is trained using the data from all the participants except one, which is held out to test the performance of the classifier. Therefore, data from the same participant is never used for training and testing simultaneously. We implemented this cross-validation strategy because it contributes to avoiding bias and serves as a robust approach for classification performance assessment. Indeed, LOSO cross-validation is the most widely adopted cross-validation strategy in the literature for the discrimination of AD groups from resting state EEG.³⁸

3. Results

3.1. Relative power analysis

Figure 3 represents, for the original 16-channel montage, the results of the statistical group comparison between the two groups for the relative power features. We split the features into five subplots corresponding to the five frequency bands where we estimated the relative power. We found statistically significant differences in the theta band (for F5) and the beta band (for Fp1, Fz, Cz, C3, C4, and P6). However, the statistical significance disappeared after applying multiple comparison correction, and only the p -values for the comparisons at Fp1, Fz, Cz, C4, and P6 in the beta band remained below 0.1.

Figure 4 represents the channel-averaged relative power in the five bands for the two study groups. For this analysis, we found statistically significant differences for the beta band. Nonetheless, statistical significance disappeared after applying multiple comparison corrections.

3.2. Complexity analysis

Figure 5 displays the results of the statistical group comparison between the two groups for the complexity features. In this case, the analysis yielded significant differences for the Hjorth complexity at Fz and Cz. However, statistical significance disappeared after applying multiple comparison correction. Alternatively, we did not find statistically significant differences for the spectral entropy in any channel.

Figure 6 shows the channel-averaged complexity features for the two study groups. For this analysis, we did not find any statistically significant differences between the two groups.

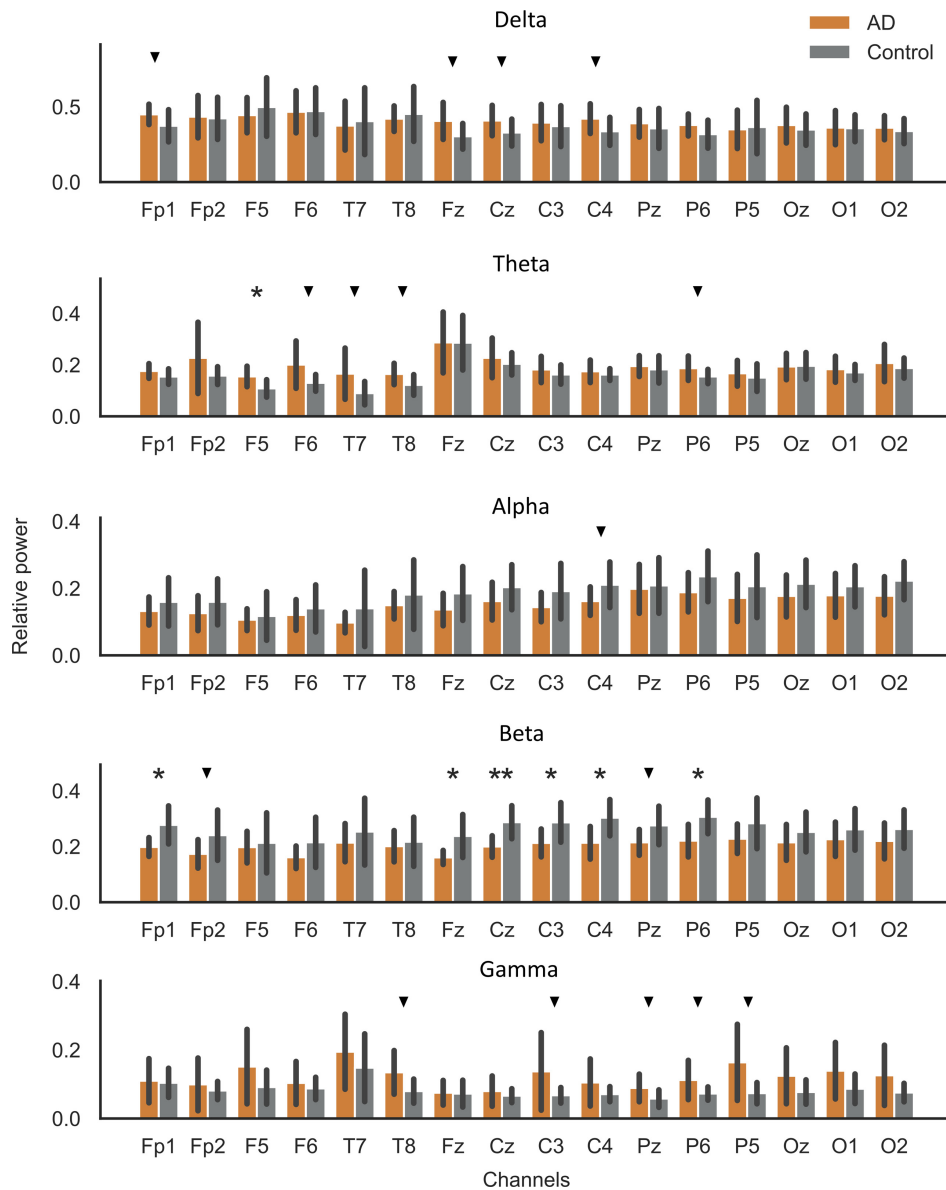


Fig. 3. Comparison of the relative power features for the two study groups using the original 16-channel montage. Each chart shows the results for a frequency band. The bars and error bars represent the mean and the standard deviation of the samples, respectively. ▼ indicates close to significant (p -value ≤ 0.15), * indicates p -value ≤ 0.05 , and ** indicates p -value ≤ 0.01 . The statistical significance disappeared after applying multiple comparison correction. Only the p -values for the comparisons at Fp1, Fz, Cz, C4, and P6 in the beta band remained below 0.1.

3.3. Channel selection for reduced montage

Figure 7 represents the different elements of the channel selection for the reduced montage: the univariate score per feature, the accumulated univariate score per channel, and the topographic representation of the accumulated scores. The highest ranked features belonged to the beta band, and the highest

ranked channels were located in the fronto-central region of the scalp.

For the reduced montage, we initially selected the top three channels in terms of accumulated feature score: Cz, Fz, and C4 (see Fig. 7(b)). Since performance was far from the original montage, we decided to add a fourth channel. First, we added P6, but average accuracy was still far from expected (0.74 ± 0.31).

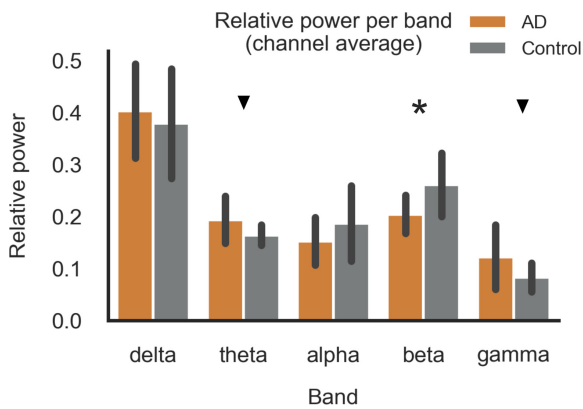


Fig. 4. Comparison of the channel-averaged relative power. The bars and error bars represent the mean and the standard deviation of the samples, respectively. ▼ indicates close to significant (p -value ≤ 0.15) and * indicates p -value ≤ 0.05 . The statistical significance disappeared after applying multiple comparison correction.

Since multiple works have shown the importance of using channels from both hemispheres,^{22,47,62} we replaced P6 with the next channel from the left hemisphere in the ranking, Fp1. In this case, mean accuracy improved (0.78 ± 0.32) but remained clear

of the expected performance. Finally, replacing Fp1 with C3, resulted in a performance similar to the original montage (0.86 ± 0.20) and also a very convenient arrangement for a minimal wearable EEG headset.

3.4. Classification performance

Table 1 shows the hyperparameters that yielded the best classification performance for the three classifiers assessed in this work. Although the classification performance was similar among the classifiers, the highest accuracy was achieved using logistic regression, and multi-layer perceptron for the original montage (0.87 ± 0.23), and the reduced montage (0.86 ± 0.20), respectively. We also performed a permutation analysis to find the chance level of the classifiers for both montages. To do so, for 10 different permutations, we randomized the labels of the dataset and we performed cross-validation. The average permutation accuracy for the original and reduced montages were 0.48 ± 0.04 and 0.51 ± 0.01 (mean \pm std.), respectively. For the rest of this subsection, the results reported in refer to those obtained with the best classifier for each of the two montages assessed in this study.

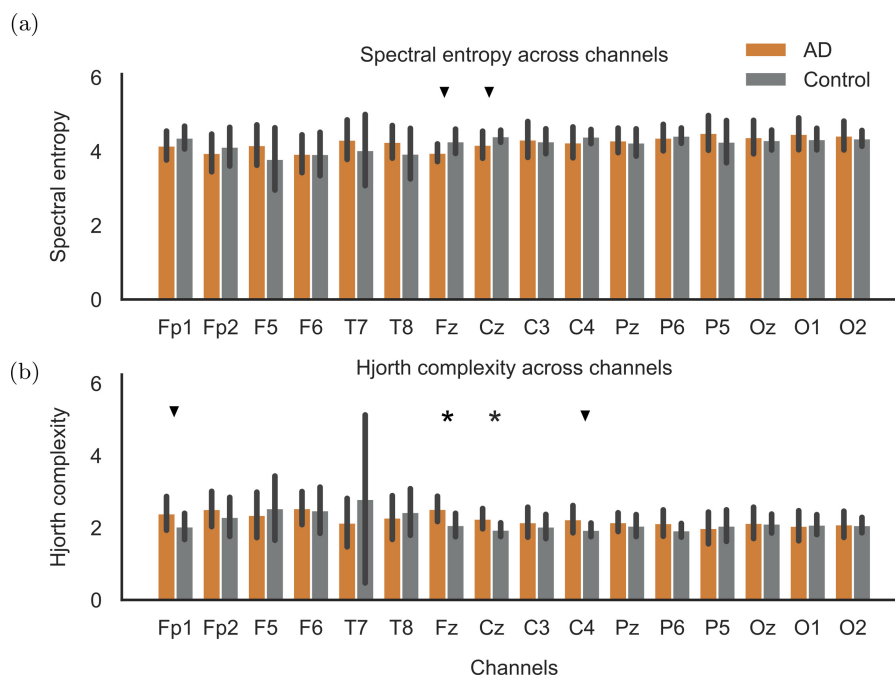


Fig. 5. Comparison of spectral entropy (a) and Hjorth complexity (b) for the two study groups using the original 16-channel montage. The bars represent the mean of the feature, and the error bars indicate the standard deviation. ▼ indicates close to significant (p -value ≤ 0.15) and * indicates p -value ≤ 0.05 . The statistical significance disappeared after applying multiple comparison correction.

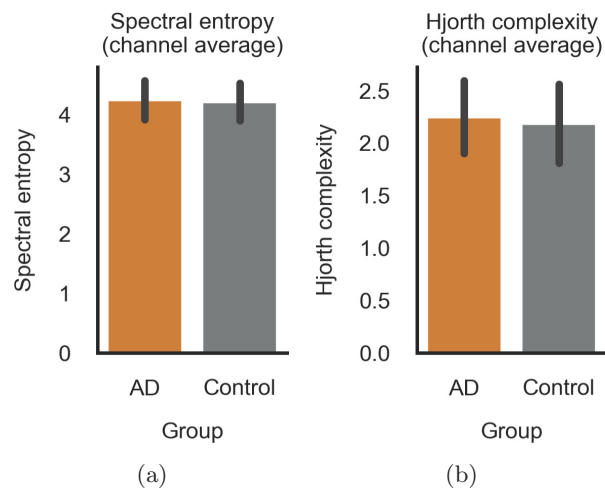
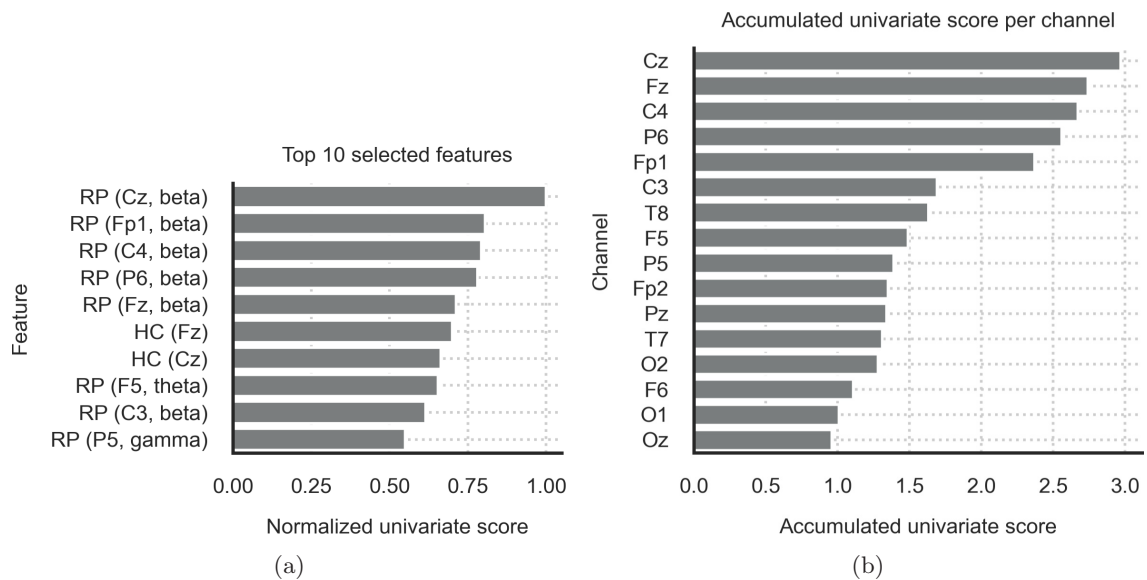


Fig. 6. Comparison of the complexity features averaged across channels for the two study groups. Bars and error bars indicate the mean and the standard deviation, respectively.



Topomap of the accumulated feature score

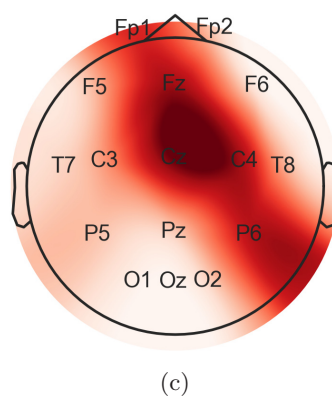


Fig. 7. (a) Top 10 features ranked by normalized univariate score. (b) Accumulated univariate feature score per channel. (c) Topographical representation of the accumulated univariate feature score per channel.

Table 1. Results of the grid-search cross-validation in terms of best hyperparameters found for each classifier and the corresponding accuracy for each of the two montages evaluated in this work. Accuracy is reported as mean \pm standard deviation.

Classifier	Hyperparameter	Best value (original montage)	Best value (reduced montage)	Accuracy (original montage)	Accuracy (reduced montage)
LR	C	10^4	1		
	class weight	balanced	balanced	0.87 ± 0.23	0.82 ± 0.27
	penalty	12	12		
SVM	C	100	100		
	gamma	auto	auto	0.87 ± 0.27	0.82 ± 0.29
MLP	activation	tanh	relu		
	alpha	10^{-3}	10^{-8}	0.85 ± 0.22	0.86 ± 0.20
	Hidden layers	10–10	3–3		

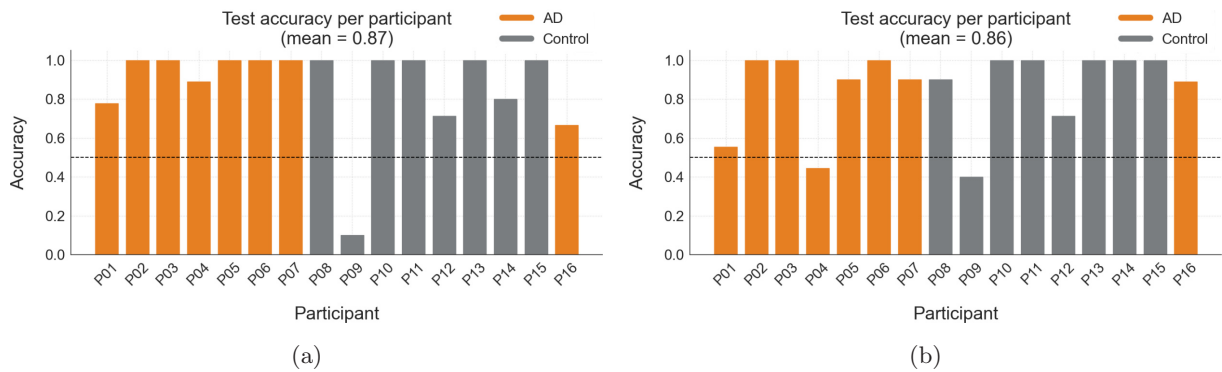


Fig. 8. Test accuracy for all the cross-validation iterations. Black dashed line represents the 0.5 chance accuracy level. (a) Original montage; (b) Reduced montage. We did not find statistically significant differences between the results yielded by the two montages.

Figure 8 represents the test accuracy per cross-validation iteration for the original and the reduced montage. The Mann–Whitney test that we applied to compare the accuracy distributions for both montages yielded a p -value equal to 0.66. Therefore, there were no statistically significant differences between the performance of the two montages.

Table 2 shows the confusion matrices at the epoch level and the participant level for the original and the reduced montages. For the epoch-level matrix, we grouped all the true labels and their corresponding predictions for the test sets of all the cross-validation iterations, and we calculated the class accuracy. For the participant level matrix, we followed a more clinically oriented approach: we considered the classifier correctly predicted the label of a participant if it correctly classified more than 50% of their epochs. This latter approach has been reported in the literature

Table 2. Confusion matrices at the epoch and the participant levels for the original and the reduced montage.

Level	Group	Montage			
		Original		Reduced	
		AD	Control	AD	Control
Epoch	AD	0.92	0.08	0.83	0.17
	Control	0.17	0.83	0.12	0.88
Participant	AD	8	0	7	1
	Control	1	7	1	7

because it represents a more realistic scenario in terms of clinical detection.

Finally, Fig. 9 displays the receiver operating characteristic (ROC) curves corresponding to the two montages evaluated in this work. For each

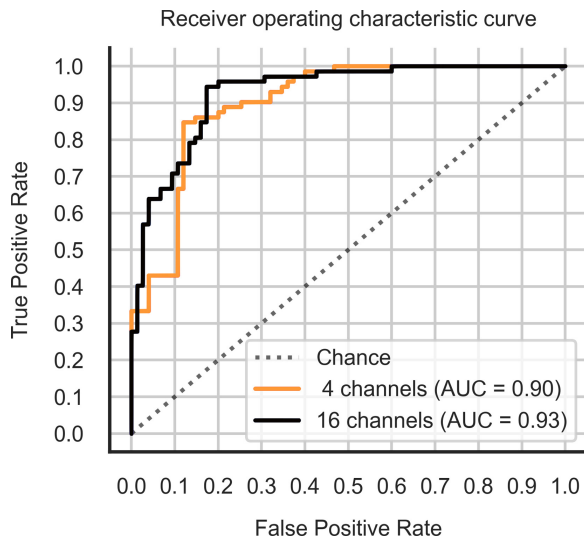


Fig. 9. ROC curves for the original 16-channel and the reduced four-channel montages. The area under the curve (AUC) is reported in the figure legend.

montage, we estimated the curve from the cross-validation predictions scored by the best classifier (see Table 1).

4. Discussion

4.1. Group differences in relative power and complexity

With respect to the relative power analysis displayed in Fig. 3, we found different patterns for each of the bands. For the delta band, the results suggest an increase in relative power for the AD group compared with the controls at the left prefrontal (Fp1), frontal (Fz), and central (Cz and C4) regions. With respect to the theta band, we found a statistically significant increase for the AD group at the left frontal region (F5), and a close to significant increase at the right frontal (F6), temporal (T7 and T8), and right posterior (P6) regions. Conversely, for the alpha band, we observe a close to significant decrease in the relative power for the AD group at the right central region (C4). The eyes open condition adopted during the resting state acquisition may be the reason behind the lack of differences in this frequency band. Alternatively, for the beta band, we observe a statistically significant decrease in the relative power for the AD group at the left prefrontal (Fp1), frontal (Fz), central (Cz, C3, and C4), and right posterior (P6) regions. The preliminary results obtained for

these four bands agree with the slowing effect widely reported in the literature^{58,63} and described in Sec. 2.3. Nonetheless, since some of the results discussed were only close to significant, they need to be taken with caution. Interestingly, the results for the gamma band suggest an increase in the relative power for the AD group in the right temporal (T8), left central (C3), and posterior (Pz, P6, and P5) regions. Although the results reported in the literature for this band are conflicting, some works have reported this same trend.^{64,65}

The differences between the AD and control groups are more evident for certain channels, which could be indicative of their higher potential to discriminate the two groups. Furthermore, for the average of the relative power across channels (see Fig. 4), we only found statistically significant differences for the beta band and close to significant differences for the theta and gamma bands. The reason behind this may be the inter-channel differences as well as the statistical effects resulting from the reduced sample involved for this study. Furthermore, the results in terms of the relative power discussed previously need to be interpreted with caution, since the statistical significance results found disappeared after correcting for multiple comparisons.

Regarding the complexity analysis, we observe opposite behaviors for the spectral entropy and the Hjorth complexity according to the results displayed in Fig. 5. This implies that the results obtained for both metrics are consistent, since sample entropy and Hjorth complexity augment with complexity and regularity, respectively. For the spectral entropy (see Fig. 5(a)), we found a close to significant decrease for the AD group in the frontal (Fz) and central (Cz) regions. Since these differences between the two groups were not statistically significant, they need to be carefully considered. Alternatively, for the Hjorth complexity, we observed the expected inverted pattern (see Fig. 5(b)). Particularly, we found a statistically significant increase for the AD group at the frontal (Fz) and central (Cz) regions. This matches the close to significant results obtained for the sample entropy for those same channels. In addition, we also found a close to significant increase for the AD group at the left prefrontal (Fp1) and right central (C4) regions. In conclusion, the results obtained for the complexity analysis, suggest a pattern of complexity reduction for the AD group with respect to

the controls. This is reflected by a decrease in sample entropy and an equivalent increase in Hjorth complexity. Such results agree with the prevailing view in the literature regarding EEG complexity in AD patients. This view supports a reduction in the EEG complexity as a result of the progressive loss of neural connections observed in the AD patients.^{32,58,66,67} Nonetheless, these results need to be carefully considered as the statistical significance found for the Hjorth complexity disappeared after correcting for multiple comparisons. Furthermore, the heterogeneity of the dementia symptoms may lead to different neurological changes in different individuals.²³ This, together with the heterogeneity of the metrics utilized to evaluate complexity, hinder the comparison between the results reported in the literature.

With respect to the average across channels for the complexity metrics (see Fig. 6), we observe a lack of statistical significance for the differences between the two groups. We believe that the reason behind this may be the reduced sample size involved for this study.

4.2. Conventional EEG montage versus reduced montage for AD detection

The main aim of this work was to investigate a reduced montage based on wearable EEG for the detection of early AD. The results that we obtained suggest that a reduced four-channel montage may feasibly support early-stage AD detection.

For this, we estimated a normalized feature score for each feature (Fig. 7(a)), then we accumulated these scores by channel (Fig. 7(b)) as a measure of their relevance and presented them in a topographical map (Fig. 7(c)). According to this analysis, the four channels with the highest accumulated score were: Cz, Fz, C4, and P6. However, we deemed this channel distribution impractical for a low-cost plug-and-play wearable system (e.g. similar to a music headset). Consequently, upon checking that performance was not noticeably affected, we replaced P6 with C3, a channel with a fairly high score (see Fig. 7(b)) and that allowed a symmetrical four-channel montage (Cz, Fz, C4, and C3). The resulting montage is in agreement with studies where channels from the two hemispheres were utilized.^{22,47,62}

Regarding the classifiers explored in this study, according to the results presented in Table 1, the

three classifiers yielded sound performance under both montages. In fact, the lowest inter-class accuracy was 0.82 while the highest was 0.87. Concretely, for the original and the reduced montage, the classifiers that yielded the highest inter-class accuracy were the LR (0.87 ± 0.23) and the MLP (0.86 ± 0.20), respectively.

Upon the results shown in Table 2, the performance of the two montages in terms of the confusion matrices (at the epoch and the participant levels) was comparable. At the epoch level, with the original montage, we obtained classification accuracies of 0.92 and 0.83 for the AD and the control classes, respectively. Alternatively, with the reduced montage, we obtained accuracies of 0.83 and 0.88. On the other hand, at the participant level, using the original montage, 8 out of 8 and 7 out of 8 participants were correctly detected for the AD and the control classes, respectively. Using the reduced montage, the performance for the AD class slightly dropped to 7 out of 8, while those for the control class remained equal. This is clearly noticeable in the cross-validation results displayed in Fig. 8: for the original montage, the classifier only misclassified more than 50% of the epochs for one participant, whilst for the reduced montage, this happened for two participants. Likewise, the ROC curves shown in Fig. 9, provide additional evidence of the similarity between the performance corresponding to both montages (with a slightly higher AUC for the original montage).

In fact, the statistical comparison between the cross-validation results for the two montages yielded a p -value equal to 0.66, which is far above the significance threshold. This implies that the cross-validation accuracy was analogous for the two montages.

In relation to other studies, the reduced montage approach presented in this work yielded a classification accuracy comparable to analogous works in the literature,^{68–70} superior^{47,62,71} in some cases, and inferior in others.^{20,21,23,72} In terms of channel number, most of the published works considered between 17 and 32 channels, with typical including 16,^{17,72} 19,^{21,22,47,69–71} or 32.^{23,73,74} Alternatively, the montage that we propose includes only four channels, which represents an important asset in terms of preparation time and patient comfort. Regarding the cross-validation strategy, we applied LOSO because

we believe that this is the strategy that better represents the patient screening procedure, as data from the same participant is not used for training and testing simultaneously. Although most studies in the literature adhered to this strategy,³⁸ other works followed a k -fold^{20,70,75} strategy, which undermines the robustness of the classifier when clinical cohorts are handled.⁷⁶ Lastly, with regard to artifact processing, in this work we applied two automated techniques: Autoreject and automated ICA. This represents a potential benefit in terms of time and costs compared to traditional approaches based on visual inspection, since no additional trained personnel is required to perform a manual epoch selection.

In view of the results discussed in the previous subsections, we believe that the approach proposed in this work can contribute to opening the door for accessible support tools aimed at the detection of early-stage AD in the clinical practice, for example, a low-cost plug-and-play device in the form of a headband.

4.3. Limitations of the study

Although the results discussed in the previous subsections are promising, this study also presents some limitations. First, the conclusions drawn in this work need to be cautiously taken given the reduced sample size. In fact, after applying correction for multiple comparisons, the significance of the results disappeared for the relative power and the complexity analyses, which was expected in view of the reduced sample size. To validate our reduced montage approach, further studies should reproduce the procedures presented in this preliminary work on a larger sample. Additionally, we used the original 16-channel montage to perform the ICA decomposition. This implies that a new blink artifact rejection approach must be considered for a potential future application of the reduced montage proposed in this work. Regarding this, since the experimental session included a personal interview, a cognitive evaluation, setting up the 16-channel EEG montage, and the EEG resting state acquisition, we conducted the latter stage under eyes-open resting state to avoid drowsiness. In a potential future application of our approach, we could perform the acquisition under eyes-closed resting state because the consulting session would be substantially shorter than an

experimental session, which would remove the need for blink artifact processing. Indeed, whilst eyes-closed resting state has been thoroughly applied in the literature, some studies have investigated the acquisition during eyes-closed resting state or during certain cognitive tasks and have obtained varying results.^{23,66,77} Hence, the comparison of different recording conditions is key to finding the best possible balance between patient comfort and detection accuracy. Furthermore, due to the recruiting strategy, the patients taking part in this work do not represent a fully realistic sample of the population under study. The patients who attend health-care services sometimes suffer from multiple neurological pathologies and they are often under medical treatment. However, following the trend in literature, we involved patients who were diagnosed only with AD and who were not under a medical treatment that could interfere with their cognitive status. This is an ineluctable challenge that needs to eventually be confronted to effectively transfer these research approaches to practice. Finally, clinical techniques like CSF analysis or PET, enable the identification of structures linked to AD, such as amyloid plaques, which is part of the procedures established to deliver a clinical diagnosis. Evidently, the approach presented in this paper cannot unveil such information, nonetheless, it may represent a fast minimal supporting tool for the detection of the disease prior to the application of clinically accepted techniques.

5. Conclusions

In a previous work, we demonstrated that early-stage AD can be detected using a simplified EEG montage during a resting state acquisition. In this paper, we extended that work by statistically analyzing the differences in EEG relative power and complexity between AD patients and controls. We estimated a feature score based on the statistical differences between the two study groups (AD and controls). The top 10 statistically different features were relative power in the beta band at Cz, Fp1, C4, P6, and Fz, Hjorth complexity at Fz and Cz, and relative power in theta at F5, in beta at C3, and in gamma at P5. Then, we estimated the accumulated feature score per channel to elucidate the four-channel selection to create a reduced montage. Finally, we compared the performance of the reduced four-channel

and the original 16-channel montages through different classifiers. The preliminary results that we obtained support our hypothesis that a reduced EEG montage could be used for supporting early-stage AD detection. With this in mind, we envision a scenario where early-stage AD can be screened within minutes in primary care services using a four-channel plug-and-play wearable system. Such approach may represent a valuable supporting tool prior to the application of standard clinical techniques. Eventually, this could contribute to reducing screening costs and to increasing the accessibility to EEG-based early-stage AD analysis, especially in the context of crowded healthcare systems or rural environments. Nonetheless, additional studies are required to validate this approach on a larger sample size and to evaluate the detection of other stages of the disease. For instance, longitudinal studies involving preclinical AD patients may bring important insights regarding the detection of prodromal stages of the disease.

Acknowledgments

The authors would like to acknowledge the members and patients of the Cognitive and Behavioral Neurology Unit at Hospital Universitario Virgen de las Nieves de Granada who took part in the study. This research was supported by Projects B-TIC-352-UGR20 and Excellence Research P21_00084 (Junta de Andalucía), PGC2018-098813-B-C31, PGC2018-098813-B-C32, PID2021-128529OA-I00 (MCIN/AEI/10.13039/501100011033 and by ERDF A way of making Europe) and the Postdoctoral Fellowship Programme of Junta de Andalucía (PAIDI 2020).

References

1. C. Patterson, *World Alzheimer Report 2018*, <https://apo.org.au/node/260056> (2018).
2. E. Perez-Valero, J. Minguillon, C. Morillas, F. Pelayo and M. A. Lopez-Gordo, Detection of Alzheimer's disease using a four-channel EEG Montage, in *Artificial Intelligence in Neuroscience: Affective Analysis and Health Applications*, eds. J. M. Ferrández Vicente, J. R. Álvarez-Sánchez, F. de la Paz López and H. Adeli (Springer International Publishing, New York, 2022), pp. 436–445, doi:10.1007/978-3-031-06242-1.
3. S. Palmqvist *et al.*, Detailed comparison of amyloid PET and CSF biomarkers for identifying early Alzheimer disease, *Neurology* **85** (2015) 1240–1249.
4. G. S. Bloom, Amyloid- β and Tau: The trigger and bullet in Alzheimer disease pathogenesis, *JAMA Neurol.* **71** (2014) 505–508.
5. J. Huang, P. Beach, A. Bozoki and D. C. Zhu, Alzheimer's disease progressively reduces visual functional network connectivity, *J. Alzheimer's Dis. Rep.* **5** (2021) 549–562.
6. M. Zvěřová, Clinical aspects of Alzheimer's disease, *Clin. Biochem.* **72** (2019) 3–6.
7. R. J. Perrin, A. M. Fagan and D. M. Holtzman, Multimodal techniques for diagnosis and prognosis of Alzheimer's disease, *Nature* **461** (2009) 916–922.
8. M. Riemenschneider *et al.*, Cerebrospinal fluid tau and beta-amyloid 42 proteins identify Alzheimer disease in subjects with mild cognitive impairment, *Arch. Neurol.* **59** (2002) 1729–1734.
9. H. Zetterberg, L.-O. Wahlund and K. Blennow, Cerebrospinal fluid markers for prediction of Alzheimer's disease, *Neurosci. Lett.* **352** (2003) 67–69.
10. J. M. Górriz, F. Segovia, J. Ramírez, A. Lassi and D. Salas-Gonzalez, GMM based SPECT image classification for the diagnosis of Alzheimer's disease, *Appl. Soft Comput.* **11** (2011) 2313–2325.
11. S. H. Hojjati, A. Ebrahimzadeh, A. Khazaei and A. Babajani-Feremi, Predicting conversion from MCI to AD using resting-state fMRI, graph theoretical approach and SVM, *J. Neurosci. Methods* **282** (2017) 69–80.
12. S. R. Meikle, F. J. Beekman and S. E. Rose, Complementary molecular imaging technologies: High resolution SPECT, PET and MRI, *Drug Discov. Today Technol.* **3** (2006) 187–194.
13. D. Pan *et al.*, Early detection of Alzheimer's disease using magnetic resonance imaging: A novel approach combining convolutional neural networks and ensemble learning, *Front. Neurosci.* **14** (2020) 259.
14. C. Babiloni *et al.*, Functional cortical source connectivity of resting state electroencephalographic alpha rhythms shows similar abnormalities in patients with mild cognitive impairment due to Alzheimer's and Parkinson's diseases, *Clin. Neurophysiol.* **129** (2018) 766–782.
15. Z. S. Nasreddine *et al.*, The Montreal cognitive assessment, MoCA: A brief screening tool for mild cognitive impairment, *J. Am. Geriatr. Soc.* **53** (2005) 695–699.
16. I. Arevalo-Rodríguez *et al.*, Mini-mental state examination (MMSE) for the early detection of dementia in people with mild cognitive impairment (MCI), *Cochrane Database Syst. Rev.* **7** (2021) CD010783.
17. N. N. Kulkarni and V. K. Bairagi, Extracting salient features for EEG-based diagnosis of Alzheimer's disease using support vector machine classifier, *IETE J. Res.* **63** (2017) 11–22.
18. M. S. Mendiondo, J. W. Ashford, R. J. Kryscio and F. A. Schmitt, Modeling mini mental state

- examination changes in Alzheimer's disease, *Stat. Med.* **19** (2000) 1607–1616.
19. H. Adeli, S. Ghosh-Dastidar and N. Dadmehr, A spatio-temporal wavelet-chaos methodology for EEG-based diagnosis of Alzheimer's disease, *Neurosci. Lett.* **444** (2008) 190–194.
 20. C. Ieracitano, N. Mammone, A. Hussain and F. C. Morabito, A novel multi-modal machine learning based approach for automatic classification of EEG recordings in dementia, *Neural Netw.* **123** (2020) 176–190.
 21. L. R. Trambaiolli, N. Spolaôr, A. C. Lorena, R. Anghinah and J. R. Sato, Feature selection before EEG classification supports the diagnosis of Alzheimer's disease, *Clin. Neurophysiol.* **128** (2017) 2058–2067.
 22. S. J. Ruiz-Gómez *et al.*, Automated multiclass classification of spontaneous EEG activity in Alzheimer's disease and mild cognitive impairment, *Entropy* **20** (2018) 35.
 23. J. C. McBride *et al.*, Spectral and complexity analysis of scalp EEG characteristics for mild cognitive impairment and early Alzheimer's disease, *Comput. Methods Programs Biomed.* **114** (2014) 153–163.
 24. K. D. Tzamourta *et al.*, EEG window length evaluation for the detection of Alzheimer's disease over different brain regions, *Brain Sci.* **9** (2019) 81.
 25. B. Oltu, M. F. Akşahin and S. Kibaroglu, Investigation of EEG signal for diagnosis of mild cognitive impairment and Alzheimer's disease, in *2019 Medical Technologies Congress (TIPTEKNO)* (IEEE, 2019), pp. 1–4, doi:10.1109/TIPTEKNO.2019.8895256.
 26. P. M. Rodrigues *et al.*, Lacsogram: A new EEG tool to diagnose Alzheimer's disease, *IEEE J. Biomed. Health Inform.* **25** (2021) 3384–3395.
 27. J. P. Amezcua-Sanchez, A. Adeli and H. Adeli, A new methodology for automated diagnosis of mild cognitive impairment (MCI) using magnetoencephalography (MEG), *Behav. Brain Res.* **305** (2016) 174–180.
 28. C. Gómez *et al.*, Synchrony analysis of spontaneous MEG activity in Alzheimer's disease patients, in *2012 Annual Int. Conf. IEEE Engineering in Medicine and Biology Society* (IEEE, 2012), pp. 6188–6191, doi:10.1109/EMBC.2012.6347407.
 29. S. Pusil, S. I. Dimitriadis, M. E. López, E. Pereda and F. Maestú, , Aberrant MEG multi-frequency phase temporal synchronization predicts conversion from mild cognitive impairment-to-Alzheimer's disease, *NeuroImage Clin.* **24** (2019) 101972.
 30. D. A. Blanco-Mora, Y. Almeida, C. Vieira and S. B. Badia, A study on EEG power and connectivity in a virtual reality bimanual rehabilitation training system, in *2019 IEEE Int. Conf. Systems, Man and Cybernetics (SMC)* (IEEE, 2019), pp. 2818–2822, doi:10.1109/SMC.2019.8914190.
 31. D. Kim and K. Kim, Detection of early stage Alzheimer's disease using EEG relative power with deep neural network, in *2018 40th Annual Int. Conf. IEEE Engineering in Medicine and Biology Society (EMBC)* (IEEE, 2018), pp. 352–355, doi:10.1109/EMBC.2018.8512231.
 32. A. H. H. Al-Nuaimi, E. Jammeh, L. Sun and E. Ifeachor, Complexity measures for quantifying changes in electroencephalogram in Alzheimer's disease, *Complexity* **2018** (2018) 1–12.
 33. J. P. Amezcua-Sanchez, N. Mammone, F. C. Morabito and H. Adeli, A new dispersion entropy and fuzzy logic system methodology for automated classification of dementia stages using electroencephalograms, *Clin. Neurol. Neurosurg.* **201** (2021) 106446.
 34. J. delEtoile and H. Adeli, Graph theory and brain connectivity in Alzheimer's disease, *Neuroscientist* **23** (2017) 616–626.
 35. N. Mammone, C. Ieracitano, H. Adeli, A. Bramanti and F. C. Morabito, Permutation Jaccard distance-based hierarchical clustering to estimate EEG network density modifications in MCI subjects, *IEEE Trans. Neural Netw. Learning Syst.* **29** (2018) 5122–5135.
 36. C. Porcaro, F. Vecchio, F. Miraglia, G. Zito and P. M. Rossini, Dynamics of the 'cognitive' brain wave P3b at rest for Alzheimer dementia prediction in mild cognitive impairment, *Int. J. Neural Syst.* **32** (2022) 2250022.
 37. M. Cecchi *et al.*, A clinical trial to validate event-related potential markers of Alzheimer's disease in outpatient settings, *Alzheimer's Dement. Diagn. Assess. Dis. Monit.* **1** (2018) 387–394.
 38. R. Cassani, M. Estarellas, R. San-Martin, F. J. Fraga and T. H. Falk, Systematic review on resting-state EEG for alzheimer's disease diagnosis and progression assessment, *Dis. Markers* **2018** (2018) e5174815, <https://www.hindawi.com/journals/dm/2018/5174815/>.
 39. E. Perez-Valero, M. A. Lopez-Gordo, C. Morillas, F. Pelayo and M. A. Vaquero-Blasco, A review of automated techniques for assisting the early detection of alzheimer's disease with a focus on EEG, *J. Alzheimer's Dis.* **80**(4) (2021) 1363–1376,
 40. A. Ortiz, J. Munilla, J. M. Górriz and J. Ramírez, Ensembles of deep learning architectures for the early diagnosis of the alzheimer's disease, *Int. J. Neur. Syst.* **26** (2016) 1650025.
 41. K. D. Tzamourta *et al.*, Machine learning algorithms and statistical approaches for alzheimer's disease analysis based on resting-state EEG recordings: A systematic review, *Int. J. Neural. Syst.* **31** (2021) 2130002.

42. L. Khedher *et al.*, Independent component analysis-support vector machine-based computer-aided diagnosis system for alzheimer's with visual support, *Int. J. Neur. Syst.* **27** (2017) 1650050.
43. O. K. Cura, A. Akan, G. C. Yilmaz and H. S. Ture, Detection of alzheimer's dementia by using signal decomposition and machine learning methods, *Int. J. Neural Syst.* **32** (2022) 2250042.
44. G. Mirzaei, A. Adeli and H. Adeli, Imaging and machine learning techniques for diagnosis of Alzheimer's disease, *Rev. Neurosci.* **27** (2016) 857–870.
45. J. P. Amezcua-Sanchez, N. Mammone, F. C. Morabito, S. Marino and H. Adeli, A novel methodology for automated differential diagnosis of mild cognitive impairment and the Alzheimer's disease using EEG signals, *J. Neurosci. Methods* **322** (2019) 88–95.
46. G. Mirzaei and H. Adeli, Machine learning techniques for diagnosis of alzheimer disease, mild cognitive disorder, and other types of dementia, *Biomed. Signal Process. Control* **72** (2022) 103293.
47. G. Fiscon *et al.*, Combining EEG signal processing with supervised methods for Alzheimer's patients classification, *BMC Med. Inform. Decis. Mak.* **18** (2018) 35.
48. F. Hatz *et al.*, Microstate connectivity alterations in patients with early Alzheimer's disease, *Alz. Res. Therapy* **7** (2015) 78.
49. A. Sohrabpour *et al.*, Effect of EEG electrode number on epileptic source localization in pediatric patients, *Clin. Neurophysiol.* **126** (2015) 472–480.
50. Z. Akalin Acar and S. Makeig, Effects of forward model errors on EEG source localization, *Brain Topogr.* **26** (2013) 378–396.
51. A. Lendínez González, C. Carnero Pardo, C. Iribar Ibabe, M. V. Zunzunegui Pastor and R. González Maldonado, Análisis de los ítems que componen la 'Batería Abreviada Granada de Evaluación Neuropsicológica', *Geriátrika (Madr.)* (2000) 141–154.
52. C. Carnero-Pardo, S. Lopez-Alcalde, R. F. Allegri and M. J. Russo, A systematic review and meta-analysis of the diagnostic accuracy of the Phototest for cognitive impairment and dementia, *Dement. Neuropsychol.* **8** (2014) 141–147.
53. M. J. Russo *et al.*, Diagnostic accuracy of the Phototest for cognitive impairment and dementia in Argentina, *Clin. Neuropsychol.* **28** (2014) 826–840.
54. E. Perez-Valero *et al.*, An automated approach for the detection of alzheimer's disease from resting state electroencephalography, *Front. Neuroinform.* **16** (2022) 924547.
55. E. Perez-Valero, M. Á. Lopez-Gordo, C. M. Gutiérrez, I. Carrera-Muñoz and R. M. Vílchez-Carrillo, A self-driven approach for multi-class discrimination in Alzheimer's disease based on wearable EEG, *Comput. Methods Progr. Biomed.* **220** (2022) 106841.
56. M. Jas, D. A. Engemann, Y. Bekhti, F. Raimondo and A. Gramfort, Autoreject: Automated artifact rejection for MEG and EEG data. *NeuroImage* **159** (2017) 417–429.
57. J. Minguillon, M. A. Lopez-Gordo and F. Pelayo, Trends in EEG-BCI for daily-life: Requirements for artifact removal, *Biomed. Signal Process. Contr.* **31** (2017) 407–418.
58. A. Horvath *et al.*, EEG and ERP biomarkers of Alzheimer's disease: A critical review, *Front. Biosci.* **23** (2018) 183–220.
59. C. Coronel *et al.*, Quantitative EEG markers of entropy and auto mutual information in relation to MMSE scores of probable alzheimer's disease patients, *Entropy* **19** (2017) 130.
60. Y. Benjamini and Y. Hochberg, Controlling the false discovery rate: A practical and powerful approach to multiple testing, *J. R. Stat. Soc. Ser. B (Methodol.)* **57** (1995) 289–300.
61. F. J. Fraga *et al.*, Towards an EEG-based biomarker for Alzheimer's disease: Improving amplitude modulation analysis features, in *2013 IEEE Int. Conf. Acoustics, Speech and Signal Processing* (2013), pp. 1207–1211, doi:10.1109/ICASSP.2013.6637842.
62. R. Cassani *et al.*, Towards automated electroencephalography-based Alzheimer's disease diagnosis using portable low-density devices, *Biomed. Signal Process. Contr.* **33** (2017) 261–271.
63. N. Benz *et al.*, Slowing of EEG background activity in parkinson's and alzheimer's disease with early cognitive dysfunction, *Front. Aging Neurosci.* **6** (2014), Article 314, pp. 1–6.
64. J. A. van Deursen, E. F. P. M. Vuurman, F. R. J. Verhey, V. H. J. M. van Kranen-Mastenbroek and W. J. Riedel, Increased EEG gamma band activity in Alzheimer's disease and mild cognitive impairment, *J. Neural Transm.* **115** (2008) 1301–1311.
65. J. A. van Deursen, E. F. P. M. Vuurman, V. H. J. M. van Kranen-Mastenbroek, F. R. J. Verhey and W. J. Riedel, 40-Hz steady state response in Alzheimer's disease and mild cognitive impairment, *Neurobiol. Aging* **32** (2011) 24–30.
66. P. Ghorbanian *et al.*, Exploration of EEG features of Alzheimer's disease using continuous wavelet transform, *Med. Biol. Eng. Comput.* **53** (2015) 843–855.
67. S. Simons and D. Abásolo, Distance-based Lempel–Ziv complexity for the analysis of electroencephalograms in patients with alzheimer's disease, *Entropy* **19** (2017) 129.
68. H. Aghajani, E. Zahedi, M. Jalili, A. Keikhosravi and B. V. Vahdat, Diagnosis of early alzheimer's disease based on EEG source localization and a standardized realistic head model, *IEEE J. Biomed. Health Inform.* **17** (2013) 1039–1045.
69. G. Fiscon *et al.*, Alzheimer's disease patients classification through EEG signals processing, in *2014 IEEE Symp. Computational Intelligence and*

- Data Mining (CIDM)* (IEEE, 2014), pp. 105–112, doi:10.1109/CIDM.2014.7008655.
70. F. C. Morabito *et al.*, Deep convolutional neural networks for classification of mild cognitive impaired and Alzheimer's disease patients from scalp EEG recordings, in *2016 IEEE 2nd Int. Forum on Research and Technologies for Society and Industry Leveraging a better tomorrow (RTSI)* (IEEE, 2016), pp. 1–6, doi:10.1109/RTSI.2016.7740576.
 71. L. R. Trambaiolli *et al.*, Improving Alzheimer's disease diagnosis with machine learning techniques, *Clin. EEG Neurosci.* **42** (2011) 160–165.
 72. R. Wang *et al.*, Power spectral density and coherence analysis of Alzheimer's EEG, *Cogn. Neurodyn.* **9** (2015) 291–304.
 73. A. Mazaheri *et al.*, EEG oscillations during word processing predict MCI conversion to Alzheimer's disease, *NeuroImage Clin.* **17** (2018) 188–197.
 74. S. Khatun, B. I. Morshed and G. M. Bidelman, A single-channel EEG-based approach to detect mild cognitive impairment via speech-evoked brain responses, *IEEE Trans. Neural Syst. Rehabil. Eng.* **27** (2019) 1063–1070.
 75. P. Durongbhan *et al.*, A dementia classification framework using frequency and time-frequency features based on EEG signals, *IEEE Trans. Neural Syst. Rehabil. Eng.* **27** (2019) 826–835.
 76. S. Yang, J. M. S. Bornot, K. Wong-Lin and G. Prasad, M/EEG-based bio-markers to predict the MCI and alzheimer's disease: A review from the ML perspective, *IEEE Trans. Biomed. Eng.* **66** (2019) 2924–2935.
 77. M. Ahmadi, H. Adeli and A. Adeli, New diagnostic EEG markers of the Alzheimer's disease using visibility graph, *J. Neural Transm.* **117** (2010) 1099–1109.